nature communications

Article

https://doi.org/10.1038/s41467-025-59747-6

Mapping pesticide-induced metabolic alterations in human gut bacteria

Received: 24 October 2024

Accepted: 30 April 2025

Published online: 10 May 2025

Check for updates

Li Chen[1,2], Hong Yan[3,4], Shanshan Di[5], Chao Guo[1], Huan Zhang[1,2], Shiqi Zhang[1], Andrew Gold[1], Yu Wang[6], Ming Hu[1], Dayong Wu[7], Caroline H. Johnson[3], Xinquan Wang[5] & Jiangjiang Zhu[1,2]

Pesticides can modulate gut microbiota composition, but their specific effects on it remain largely elusive. In our study, we show that pesticides inhibit or promote the growth of various gut microbial species and can be accumulated to prolong their presence in the host. Pesticide exposure also induces significant alterations in gut bacterial metabolism, as reflected by changes in hundreds of metabolites. We generate a pesticide-gut microbiota-metabolite network that not only reveals pesticide-sensitive gut bacteria species but also reports specific metabolic changes in 306 pesticide-gut microbiota pairs. Using an in vivo mouse model, we further demonstrate the interactions of a representative pesticide-gut microbiota pair and verify the inflammation-inducing effects of pesticide exposure on the host, mediated by microbially dysregulated lipid metabolism. Taken together, our findings generate a comprehensive atlas of pesticide-gut microbiota-metabolite interactions atlas and shed light on the molecular mechanisms by which pesticides affect host health via gut microbiota-modulated metabolism.

Pesticides are extensively utilized globally to meet the increasing demand for food, and for enhancing the quality of agricultural products. Consequently, concerns regarding the health risks on non-targeted organisms[1–3] or humans[4,5] associated with pesticides are arising due to their residues in soil[6], water[7], and air[8]. Human populations often encounter multiple pesticides through their dietary intake[9], drinking habits[10], or occupational exposure[11]. Meanwhile, the gastrointestinal tract, acting as a protective barrier against pathogenic microorganisms and toxins, is also a primary site for pesticide exposure, and plays a crucial role in the metabolic and immune functions of the host[12,13]. Within the gastrointestinal tract, it is well-recognized that a vast gut microbiota community of 100 trillion microbial cells forms a complex ecosystem[14], and this intricate ecosystem maintains a mutualistic relationship with its host. The stability of a healthy gut microbial composition is essential for various physiological processes, including food digestion, nutrient assimilation, immune function, and neuro-behavioral processes[15–17]. The disruption of a balanced composition, known as gut microbial dysbiosis, directly impacts the host's overall well-being, and has been linked to a spectrum of human diseases and conditions, including diabetes, asthma, obesity, Alzheimer disease and cancer[18–22].

So far, in vitro and in vivo studies have predominantly concentrated on elucidating the mechanisms of oxidative stress[23,24] as a primary connection between human pesticide exposure and various chronic diseases[25,26]. Just recently, emerging research has begun to shed light on the toxic effects of pesticides on the gut microbiota, although most of these studies are still mainly focused on observing qualitative or quantitative alterations in its composition[27–29].

[1]Human Nutrition Program, Department of Human Sciences, The Ohio State University, Columbus, OH 43210, USA. [2]James Comprehensive Cancer Center, The Ohio State University, Columbus, OH 43210, USA. [3]Department of Environmental Health Sciences, Yale School of Public Health, New Haven, CT, USA. [4]State Key Laboratory of Environmental and Biological Analysis, Hong Kong Baptist University, Hong Kong, China. [5]State Key Laboratory of Agricultural Products Safety/ Key Laboratory of Detection for Pesticide Residues and Control of Zhejiang, Institute of Agro-product Safety and Nutrition, Zhejiang Academy of Agricultural Sciences, Hangzhou 310021, China. [6]Department of Physiology, Johns Hopkins University School of Medicine, Baltimore, MD 21205, USA. [7]Department of Cancer Biology and Genetics, The Ohio State University College of Medicine, Columbus, OH 43210, USA. e-mail: zhu.2484@osu.edu

Therefore, a systematic study of the metabolic responses of gut microbiota to various pesticides is critically needed, preferably with a selection of well-recognized, health- relevant, representative gut bacteria species and the adoption of universally accepted metabolic analysis approaches for gut microbiome.

In this work, we first introduce a microbiome-focused, integrated, mass-spectrometry-based metabolomics pipeline for the metabolic characterization of gut microbes in response to pesticide exposure. Then, by leveraging multi-omics investigations, our study discovers important interactions between representative gut bacteria species and well-recognized pesticide pollutants. Finally, we extend our investigation to a mouse model to verify the interactions between gut bacteria and the host following pesticide exposure and explore the consequential health implications of these interactions.

Results

Species-specific gut bacteria response network to pesticides

To assess the impacts of pesticides on human gut microbiota, we conducted a systematic analysis of interactions between eighteen pesticides (comprising fifteen representative pesticides and three known pesticide metabolites) and seventeen representative human gut bacterial species (Supplementary Data 1 and Fig. 1a). The selection

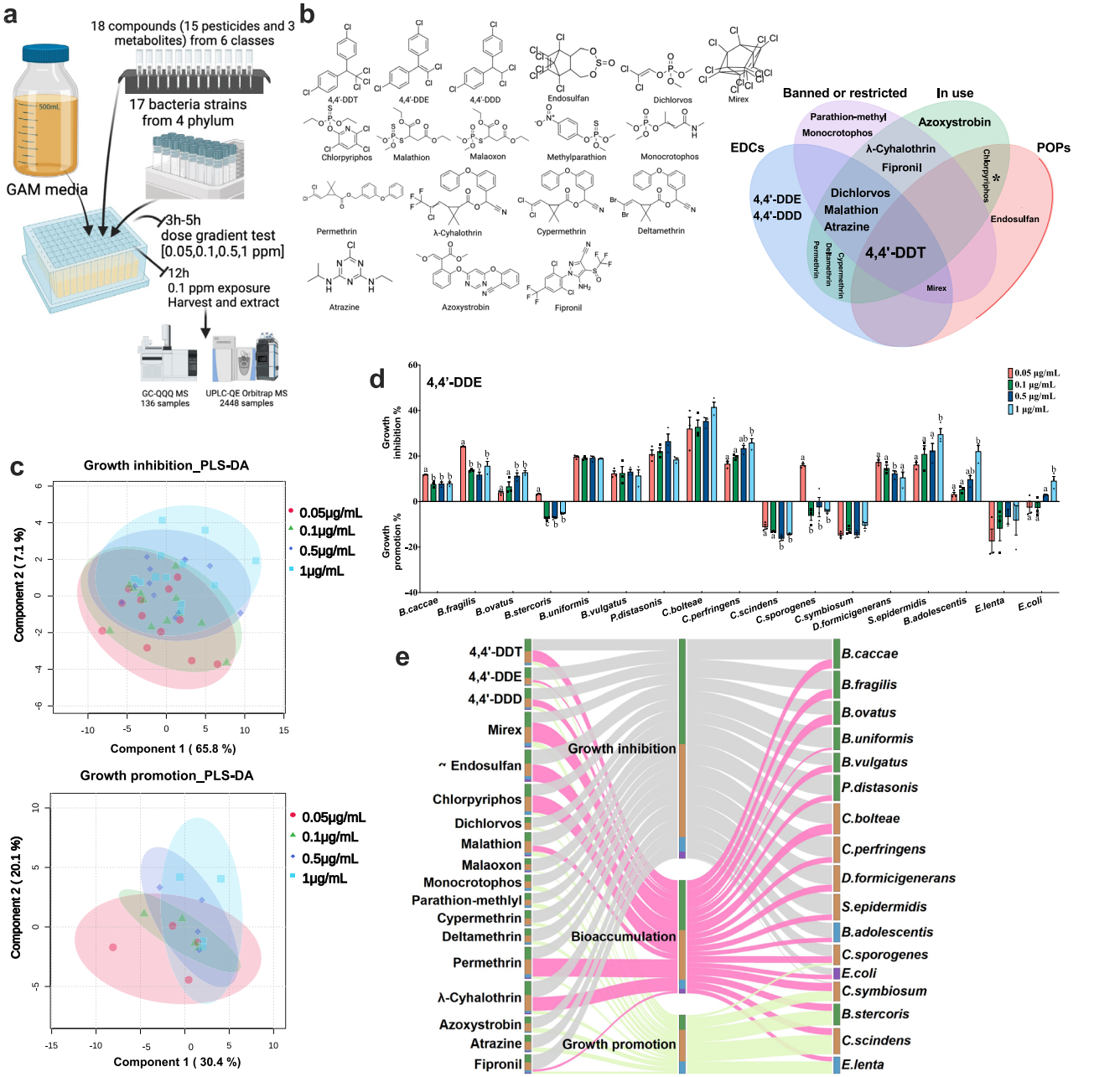

Fig. 1 | Gut bacteria accumulate pesticides without altering them. a schematic of the assay. Created in BioRender. Gold, A. (2025) https://BioRender.com/tdb7tms. **b** Structures of 18 compounds across 6 pesticide classes. **c** pesticides elicit growth effects of gut microbiota at 0.05 μg/mL, 0.1 μg/mL, 0.5 μg/mL, and 1 μg/mL. **d** 4,4′-DDE induced growth inhibition and promotion on 17 gut bacteria species under four concentrations; $n = 3$ biological replicates. **e** Bacteria-pesticide interaction network among growth inhibition/promotion and bioaccumulation in the study. Data are presented as mean ± SEM. p values were calculated by two-sided unpaired t test, and $p < 0.05$ represents statistically significant. EDCs endocrine-disrupting chemicals, GAM gifu anaerobic broth, GC-QQQ MS gas chromatography-triple quadrupole mass spectrometry, POPs persistent organic pollutants, UPLC-QE Orbitrap MS, ultra-performance liquid chromatography-quadrupole orbitrap mass spectrometry.

of pesticides was based on their widespread agricultural use globally. Among the fifteen pesticides, eleven are still used across some areas of the world, despite some being identified as endocrine-disrupting chemicals (e.g., 4,4′-DDT, atrazine, and permethrin), persistent organic pollutants (e.g., chlorphyriphos, 4,4′-DDT), or prohibited or restricted in certain countries (Fig. 1b). Noteworthy variations in maximum residue limits for specific pesticides across different products and countries have raised concerns regarding potential health risks associated with these limits (Supplementary Fig. 1a). To encompass a wide range of phylogenetic and metabolic diversity, we selected seven species from *Bacteroidetes*, seven species from *Firmicutes*, two species from *Actinobacteria*, and one species from *Proteobacteria* for initial growth inhibition/promotion experiments. *Firmicutes* and *Bacteroidetes*, which collectively account for approximately 90% of the gut microbiota, are known to play significant roles in maintaining microbial diversity[30]. Before conducting a comprehensive interaction analysis, we first measured the growth curves of gut bacterial species to assess their distinct growth rates (Supplementary Fig. S1b-r). Subsequently, we further examined the dose-dependent effects of 306 bacteria-pesticide pairs on bacterial growth inhibition or promotion across four concentration gradients during the exponential phase. Within the 0.05–1 μg/mL pesticide concentration range (Supplementary Data 2, 3 and Supplementary Fig. 1s), one Gram-negative species (*B. stercoris*) and three Gram-positive species (*E. lenta*, *C. symbiosum*, and *C. scidens*) exhibited growth promotion following pesticide exposure. On the other hand, six Gram-negative species (*B. vulgatus*, *B. ovatus*, *B. caccae*, *B. uniformis*, *B. fragilis*, and *P. distasonis*) and five Gram-positive species (*D. formicigenerans*, *C. perfringens*, *C. bolteae*, *S. epidermidis*, and *B. adolescentis*) exhibited growth inhibition.

Furthermore, we conducted a partial least squares discriminant analysis (PLS-DA) to investigate the inhibition or promotion effects of 18 compounds on growth of 17 gut bacteria species (Fig. 1c). The PLS-DA plot effectively distinguished between different pesticide concentration groups, highlighting specific concentrations with different effects on bacterial growth. This analysis provided insights into the dose-dependent relationship, revealing the environmental impact of varying pesticide concentrations on gut bacterial growth. For instance, following exposure to 4,4′-DDE at four concentrations (Fig. 1d), the growth of 11 gut bacteria species was inhibited, 3 gut bacteria species were promoted, and 3 bacteria were shown conversely dose-dependent response to this pesticide. As the pesticide concentration increased, growth inhibition intensified in *B. ovatus*, *C. perfringens*, *S. epidermidis*, *B. adolescentis*, and *E. coli*, while growth promotion strengthened in *C. scindens*. Conversely, growth inhibition decreased in *B. caccae*, *B. fragilis*, *B. stercoris*, *C. sporogenes*, and *D. formicigenerans*. Our findings reveal that bacterial responses to pesticides are both species- and dose-dependent, possibly driven by the interplay between bacterial physiology and the physiochemical properties of pesticides.

Furthermore, we investigated the capacity of gut bacteria to bioaccumulate pesticides after short-term (12-h) exposure at 0.1 μg/mL (Supplementary Fig. 2a–c). Eight of the ten detected pesticides are classified as persistent organic pollutants or endocrine-disrupting chemicals (Fig. 1b and Supplementary Fig. 2d). The ability of these pesticides to accumulate, as opposed to others, may be explained by differences in physicochemical properties (e.g., hydrophobicity and stability). For instance, organochlorine pesticides like 4,4′-DDT are known for their high lipid solubility and stability[31], which may enhance their uptake by bacterial cells. While individual pesticide levels only increased by a few percent, the combined bioaccumulation across all pesticides exceeded ten percent in *C.bolteae* and *B.ovatus* (Supplementary Fig. 2d). These bioaccumulation in gut bacteria may help explain the persistence of pesticide residues in humans. The gut bacteria-pesticide interaction network (Fig. 1e) indicated that the growth of most gut bacteria was inhibited by all pesticides, while only a few was promoted. However, our results indicated that all gut bacteria species can selectively bioaccumulate pesticides, and the ability of bioaccumulation is pesticide dependent. These results quantitatively confirmed the long-standing speculations that pesticide induced growth inhibition or promotion on gut bacteria. Our data also supported that pesticides disrupt gut microbial composition, while bacteria accumulation of pesticide increases the risk of prolonged pesticide residue in the host.

Mapping the pesticide-gut microbiome-metabolite interactions

It is often assumed that gut bacteria responses to pesticide are associated with the changes of gut bacterial metabolites, thereby regulating host health. However, experimental evaluation of these responses metabolically has not been done. To fill the gap of knowledge, we conducted high-throughput metabolomics analyses to elucidate changes in endogenous metabolites in gut bacteria species after pesticide exposure in vitro. To elucidate the mechanisms underlying the changes of microbial metabolism in response to pesticides, we first profiled over 468 (Supplementary Data 4 and Supplementary Fig. 3) metabolites from the pesticide-bacteria network interaction experiments and summarized these metabolic responses of pesticide-inhibited or promoted bacteria (Fig. 2a). We found six highly pesticide-sensitive gut bacteria exhibiting the most significant changes in terms of the number of metabolites impacted (Fig. 2a). These species include *B.ovatus*, *B.uniformis*, *D.formicigenerans*, *B.stercoris*, *C.symbiosum*, and *B.adolescentis* (Fig. 2a). We further mapped the network interactions between gut bacteria and pesticides affecting metabolites from different metabolic pathways (Fig. 2b). The significant metabolic alterations mapped into 40 metabolic pathways (Fig. 2b, c and Supplementary Data 5), encompassing important pathways such as amino acid metabolism, carbohydrate metabolism, cofactors and vitamins metabolism, nucleotide metabolism, and sulfate/sulfite metabolism (Supplementary Fig. 4). In the network visualization (Fig. 2b), Gram-positive and Gram-negative bacteria exhibited distinct metabolic responses, while pesticides formed a separate, cohesive cluster, highlighting their functional similarity in driving metabolic changes in gut bacteria. Among these pathways, the top five of most affected pathways included pyrimidine metabolism, purine metabolism, arginine and proline metabolism, lysine degradation, and phenylalanine and tyrosine metabolism (Fig. 2c). These pathways are essential for nucleotide synthesis and amino acid metabolism, both of which are fundamental to maintaining cellular and metabolic functions. At the molecular level, this highlights how pesticides can influence the growth of gut microbes. Additionally, gut microbial nucleotide and amino sugar metabolism, as part of carbohydrate metabolism, may contribute to insulin resistance in the host[32]. However, many connections between gut microbial metabolites and host health remain poorly understood. Our study provides a valuable resource to advance further research on gut microbiota-host interactions.

Next, we highlight the potential implications of our study to future research by describing the relationships between pesticide exposure and several well-known metabolic pathways of gut microbiota. Notably, we observed that pesticides directly impact tryptophan metabolism (Fig. 3a), propanoate metabolism (Fig. 3b) and bile acid metabolism (Fig. 3c) in several gut bacteria species, therefore leading to the dysregulated production of indole and its derivatives (indoles), short-chain fatty acids (SCFAs) and bile acids (BAs) which will potentially in turn modulate immune and inflammatory responses of the host[33]. It is also interesting to note that pesticides can affect the same pathways in different gut bacteria species by inducing the dysregulated production of distinct metabolites within those pathways (Fig. 3a–c). For instance, pesticides influenced tryptophan metabolism in ten gut bacteria species, and each of these impacted bacteria exhibits distinct pattern of pesticide-sensitive metabolites (Fig. 3a and

https://doi.org/10.1038/s41467-025-59747-6

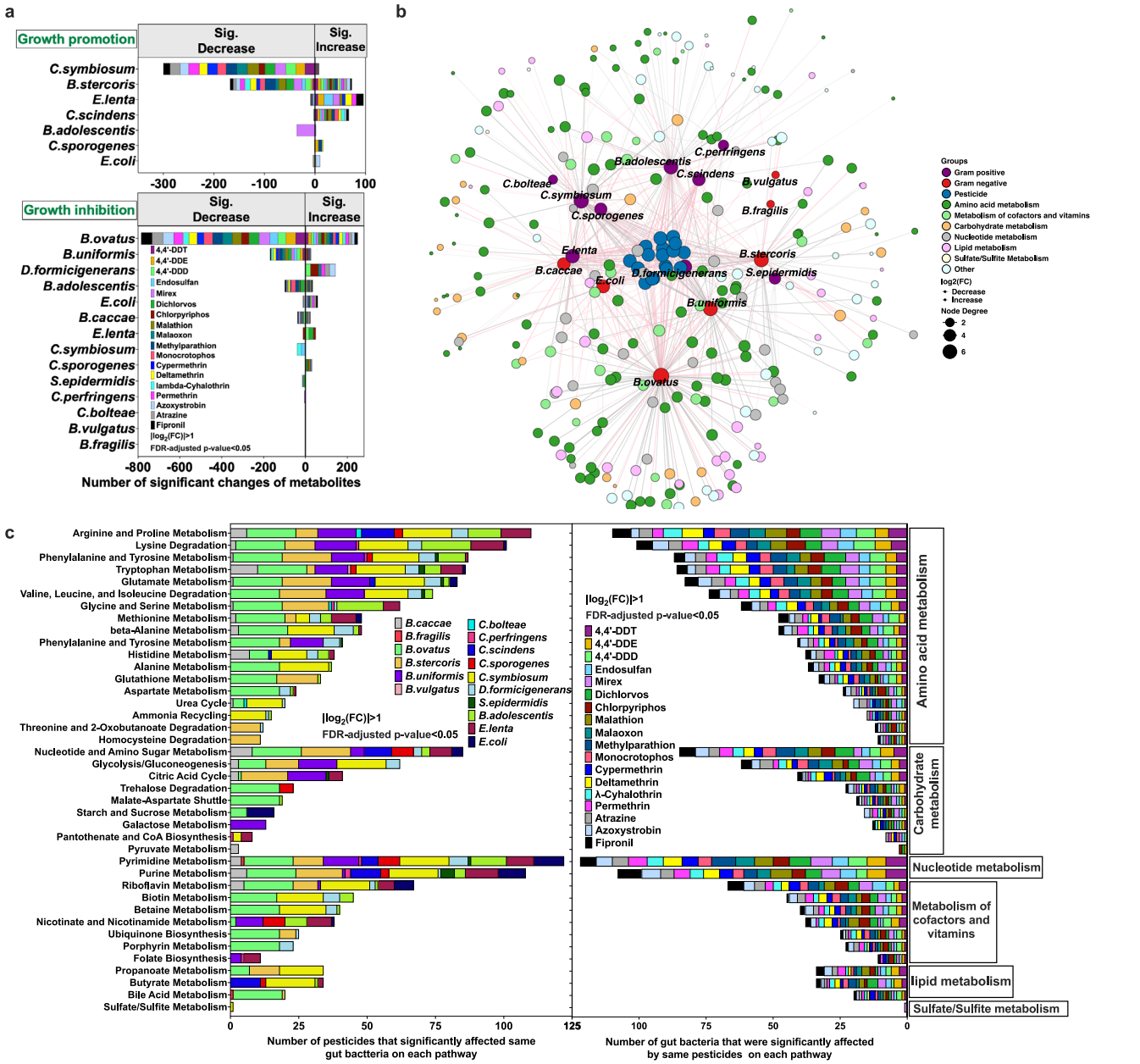

Fig. 2 | pesticide exposure led to broad and systemic changes in metabolites across gut microbiota. a Number of significant changes in metabolites for bacteria species with growth promotion or inhibition after exposure to 18 compounds. **b** Network interaction analysis between gut microbiota and pesticides affecting metabolites from different metabolic pathways. **c** Number of pesticides that significantly affected polar metabolic pathways for each bacteria strain. Data are presented as |log2(FC)| > 1 and FDR-adjusted p value < 0.05. Statistical significance was assessed using a two-sided unpaired Student's t test (**a**–**c**), with p values adjusted for multiple comparisons using the Benjamini-Hochberg method. FC fold change, FDR false discovery rate.

Supplementary Fig. 4); In *B.ovatus*, decreased L-tryptophan, N1-acetyl-N2-formyl-5-methoxykynuramine, anthranilate, trans-3-indoleacrylic acid, and increased indole, indole-3-acetic acid, indole-3-acetyl-L-alanin and 2-aminomuconic acid were observed when exposed to the tested pesticides, while we found only increased 2-amino-3,7-dideoxy-D-threo-hept-6-ulosonate in *B.vulgatus* with the same exposure experiments. Meanwhile, all pesticides can affect the tryptophan metabolism in *B.ovatus*, but only dichlorvos can affect it in *B.vulgatus* (Fig. 3a and Supplementary Fig. 4). These findings underscore the complexity of pesticide-induced metabolic alterations in gut microbes, where specificity at the pathway level remains challenging. To identify bacterial species-associated metabolites, we analyzed correlations between pesticide-induced bacterial growth perturbations and significant changes in metabolite levels. Through this approach, we identified metabolites whose levels changed significantly in association with only one gut bacterium, compared to others, following pesticide exposure. For example, S-succinyl-2,6-diaminopimelate which was positively correlated with *B. stercoris* (Fig. 3d). By linking specific metabolites to bacterial strains, our study also demonstrated the potential of developing diagnostic tools for detecting gut microbiota abnormalities through metabolite profiling during environmental exposure events. In this study, we identified pesticide-sensitive gut bacterial species, the most impacted gut microbial metabolic pathways, and bacterial species-associated metabolites. By integrating high-throughput data, we mapped critical networks of pesticide-gut microbiota-metabolite interactions, providing a comprehensive dataset to advance research on the pathogenic mechanisms underlying pesticides' effects on human health.

https://doi.org/10.1038/s41467-025-59747-6

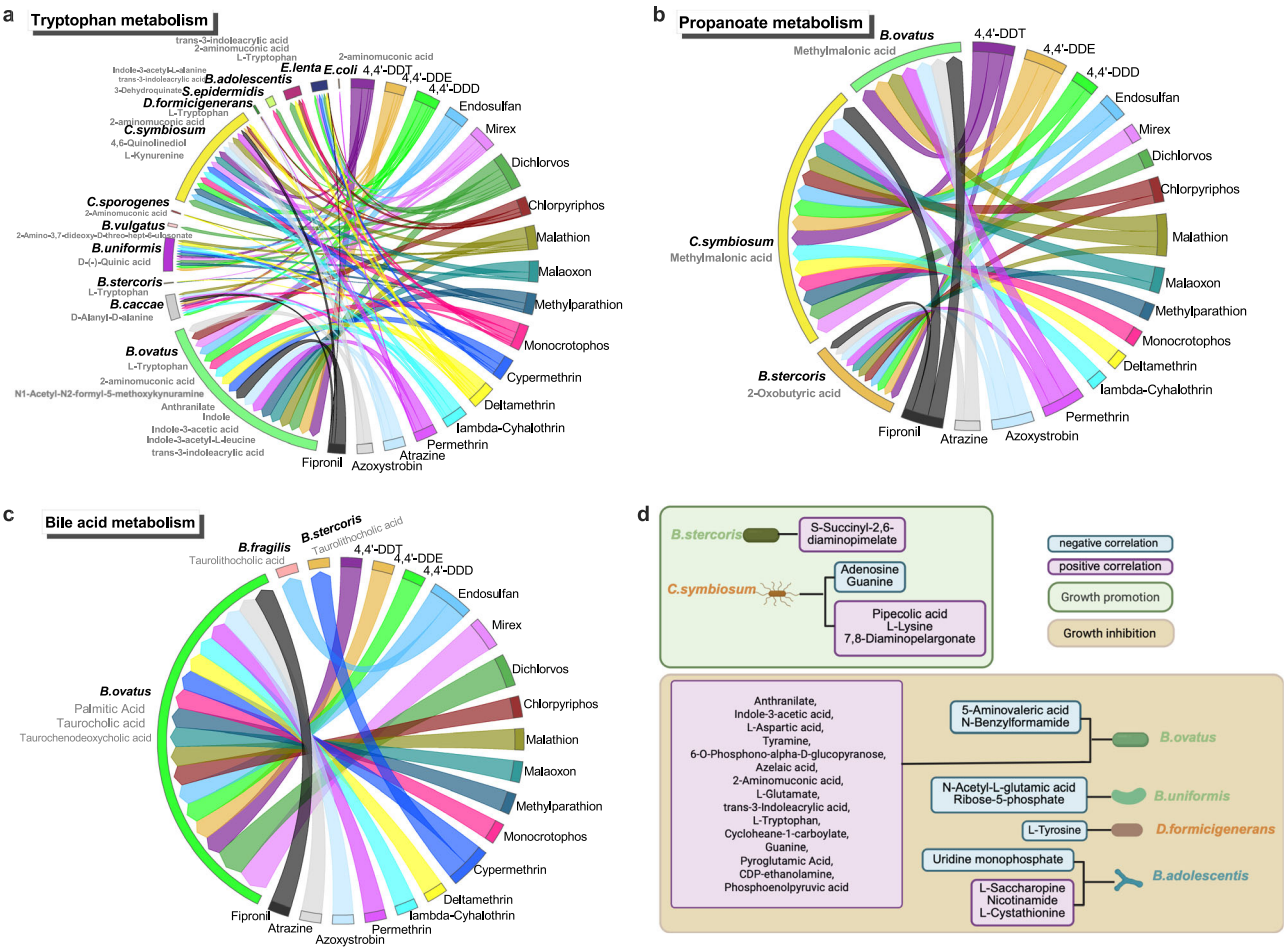

Fig. 3 | Network interaction analyses indicate that pesticide exposure led to changes in metabolites across gut microbiota. a Network interaction analysis of pesticides affected tryptophan metabolism for ten bacteria species by different metabolites. **b** Network interaction analysis of pesticides affected propanoate metabolism for three bacteria species by different metabolites. **c** Network interaction analysis of pesticides affected bile acid metabolism for three bacteria species by different metabolites. **d** Pearson correlation analysis between growth promotion/inhibition and significant changes of metabolites. Created in BioRender. Gold, A. (2025) https://BioRender.com/ym2wgf6. Data are presented as $|\log2(FC)| > 1$ and FDR-adjusted p value < 0.05. Statistical significance was assessed using a two-sided unpaired Student's t test (**a**–**d**), with p values adjusted for multiple comparisons using the Benjamini-Hochberg method. FC fold change, FDR false discovery rate.

Discovering pesticide-gut microbiome-lipids interactions

The gut microbiome is increasingly recognized as an endocrine organ, producing secretions that can influence the body through the bloodstream or lymphatic system[34]. The gut microbiome has the capacity to transform and synthesize bioactive lipids with structural and signaling functions, impacting host metabolism and immunology[35]. While our study included several known endocrine disrupting pesticides, it is plausible that undefined endocrine disruptors could also modulate the production of bioactive lipids by the gut microbiota. Therefore, we further conducted a comprehensive lipidomics analysis to investigate how pesticides affect gut bacterial lipid molecule changes and reported the pesticides-gut microbiome-lipids interaction here from various levels such as lipid categories, classes, chain lengths of fatty acyl, and saturation status (Fig. 4a, Supplementary Figs. 5–7). We also mapped the network interactions between gut bacteria and pesticides affecting lipid metabolism based on major lipid categories (Fig. 4b). In the network visualization, Gram-positive and Gram-negative bacteria exhibited distinct lipidomic responses, while clustered pesticides indicated their functional similarity in driving lipid changes in gut bacteria. Furthermore, the most significant changes in lipid categories, particularly glycerophospholipids (GPs) and glycerolipids (GLs), were predominantly associated with specific bacterial species, including *B.stercoris*, *C.scindens*, and *C.symbiosum* (Fig. 4b, c, and Supplementary Figs. 6, 7a). Overall, the most significant changes of lipids in GPs, which are expected as they are known to be abundant in bacterial cell membranes and therefore are generally at the frontier of attack by pesticides[35]. Diving into the lipid classes level (Fig. 4c, and Supplementary Figs. 6, 7b), we further observed that pesticides significantly influenced acylcarnitine (CAR, CAR 20:0) from FAs, diacylglycerol (DG, such as DG 16:1_17:1) and ether-linked diacylglycerol (EtherDG, such as DG O-16:2_17:1) from GLs, ceramide non-hydroxyfatty acid-dihydrosphingosine (Cer_NDS, such as Cer 17:0; 2 O/15:0) from SPs, and ether-linked lysophosphatidylglycerol (EtherLPG, such as PG O-17:1_16:0) from GPs in many gut bacteria and in particular in *B.stercoris*, *C.symbiosum*, and *C.scindens*.

We also discovered that, in FAs, the most significant changes in the quantity of fatty acyl chains occurred in *B.stercoris*, while saturated C20:0 significantly changed in 9 bacteria species (Fig. 4d). Therefore, the saturated fatty acid C20:0, arachidic acid, may be further considered as a sensitive bioindicator for gut bacteria following pesticide exposure. Compared to even numbered-lipids in mammals, bacterial lipids embrace greater diversity with both odd- and even-numbered fatty acyl chains reported in previous studies[36], such as C15/ C17/ C19 vs C16/ C20/ C22 in the FAs (Fig. 4d), GLs (Supplementary Fig. 7c), GPs (Supplementary Fig. 7d), and SPs (Supplementary Fig. 7e). After pesticides exposure, significant changes in the quantity of fatty acyl chains were observed in C15:0, C16:0, C17:0, and C17:1 in FAs, GLs, GPs, SPs (Fig. 4d and Supplementary Fig. 7b–d), while C28:1 and C9:0 were

https://doi.org/10.1038/s41467-025-59747-6

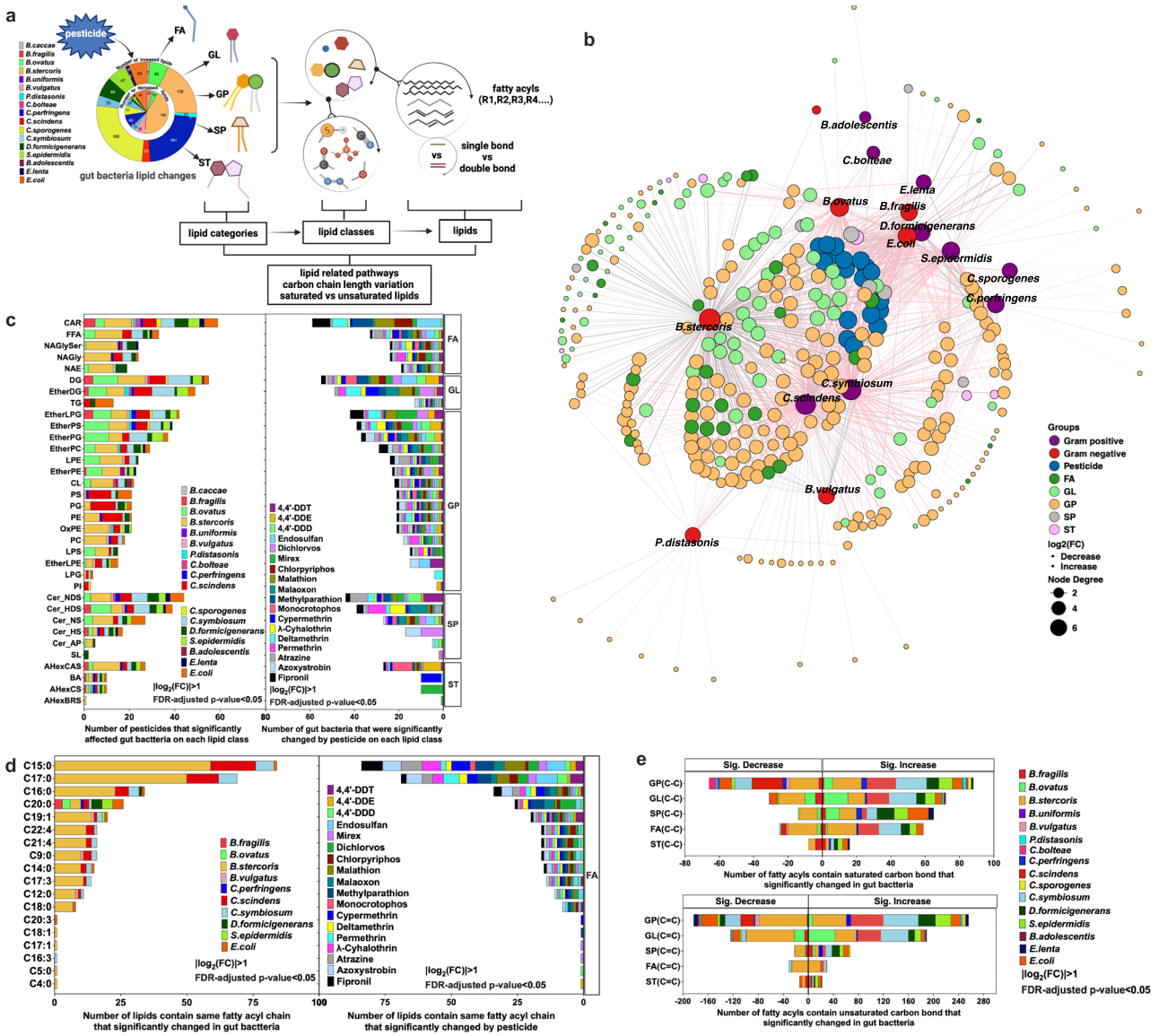

Fig. 4 | pesticide exposure induces extensive and systemic changes in lipids across gut bacteria species. a Workflow for lipid analysis including lipid categories, lipid classes and individual lipid species. Created in BioRender. Gold, A. (2025) https://BioRender.com/09x50e3. **b** Network interaction analysis between gut microbiota and pesticides affecting lipid metabolism. **c** Number of pesticides or gut bacteria species that were significantly changed on each lipid classes. **d** Number of lipids contain same fatty acyl chain that significantly changed for FA category. **e** Number of lipid carbon bond that significantly changed in gut bacteria by pesticide exposure. Data are presented as |log2(FC)| >1 and FDR-adjusted *p* value < 0.05 (**b**–**e**). Statistical significance was assessed using a two-sided unpaired Student's *t* test, with *p* values adjusted for multiple comparisons using the Benjamini-Hochberg method. AHexBRS acylhexosyl brassicasterol, AHexCAS Acylhexosyl campesterol, AHexCS acylhexosyl cholesterol, BA bile acid, CAR acylcarnitine, Cer ceramide, Cer_AP ceramide alpha-hydroxy fatty acid-phytospingosine, Cer_HS ceramide hydroxy fatty acid-sphingosine, Cer_HDS Ceramide hydroxy fatty acid-dihydrosphingosine, Cer_NDS Ceramide non-hydroxyfatty acid-dihydrosphingosine, Cer_NS Ceramide non-hydroxyfatty acid-sphingosine, CL cardiplipin, DG diacylglycerol, EtherDG Ether-linked diacylglycerol, EtherLPE Ether-linked lysophosphatidylethanolamine, EtherLPG Ether-linked lysophosphatidylglycerol, EtherPC Ether-linked phosphatidylcholine, EtherPE Ether-linked phosphatidylethanolamine, EtherPG Ether-linked phosphatidylglycerol, EtherPS Ether-linked phosphatidylserine, FA fatty acyl, FFA fatty acid, FC fold change, FDR false discovery rate, HexCer hexosylceramide alpha-hydroxy fatty acid-dihydrosphingosine, MGDG monogalactosyldiacylglycerol, GL glycerolipid, GP glycerophospholipid, LPE ether-linked lysphosphatidylethanolamine, LPG Lysophosphatidylglycerol, LPS Lysophosphatidylserine, NAE N-acyl ethanolamines, NAGly N-acyl glycine, NAGlySer N-acyl glycyl serine, NAOrn N-acyl ornithine, NATau N-acyl taurine, oxFA oxidized fatty acid, oxTG oxidized triglyceride, oxPS oxidized phosphatidylserine, PC phosphatidylcholine, PE phosphatidylethanolamine, PEtOH phosphatidylethanol, PI phosphatidylinositol, PG phosphatidylglycerol, PS phosphatidylserine, SL sulfonolipid, SM sphingomyelin, SP sphingolipid, SSulfate sterol sulfate, ST sterol lipid, TG triacylglycerol.

affected in STs (Supplementary Fig. 7f); Odd chain fatty acids (OCFAs), C15:0, C17:0 and C17:1 can be enlongated to very-long-chain FAs (VLCFAs) or can be derived from these VLCFAs[37]. Oxidation of these odd-chain FAs can yield propionyl-coenzyme A (CoA) to replenish the citric acid cycle, and the concentrations of C15:0 and C17:0 are associated with risk for multiple disease and even involved in discussions of biomarker identification and treatment targets[38]. Furthermore, C 9:0 can regulate epithelial immunological barrier function[39]. The changes for each lipid category were identified to be associated with specific gut bacteria. For example, pesticides primarily induce changes of the length of fatty acyls chains in *B.stercoris* across all lipid categories. However, in *C.symbiosum* and *C.scindens,* pesticides induced changes across GLs and GPs; in *B.stercoris*, *D.formicigenerans*, *S.epidermidis*, and *E.coli,* pesticides induced changes were observed across SPs and STs;

while in *B.fragilis*, *B.stercoris*, *B.ovatus*, and *E.coli,* changes were detected primarily in STs. Furthermore, it is well-known that lipid A (endotoxin), a component of lipopolysaccharide (LPS), is a glucosamine-based phospholipid that typically contains C14, C16 and C18 hydroxy acyl chains in most Gram-negative bacteria[40–42]. We observed significant changes in C14:0, C16:0 and C18:1 in GPs and GLs in gut bacteria, especially for Gram-negative bacteria *B.stercoris* after pesticide exposure (Supplementary Fig. 7c, d). We speculated that pesticides can disrupt the levels of those lipids in certain gut bacteria, such as *B.stercoris*, leading to a potential dysregulation of lipid A or LPS[43], and indirectly affecting the host immune system[44]. Additionally, pesticides predominantly affected lipids with carbon bond across all lipid categories (Fig. 4e and Supplementary Fig. 7g) in *B.stercoris*, *C.symbiosum*, *C.scindens*, and *E.coli*. The substantial increase in the number of saturated C-C bonds suggests that gut bacteria may be adapting to pesticide exposure through an oxidative stress response[45,46].

Pesticide drives the change of gut microbe and host metabolism in vivo

Considering the extensive effects of pesticides on gut bacteria and metabolite levels in vitro (Supplementary Fig. 8a), we further selected a representative pesticide-gut bacteria pair to explore the pesticide-gut bacteria-host interactions in vivo. Among many of the pesticide-inhibited bacteria, *B.ovatus* (a Gram-negative bacterium) was selected for the in vivo study. This study design was supported by its highest pesticide bioaccumulation (Supplementary Fig. 2d) and the largest number of significantly changed metabolites (Supplementary Fig. 8b). Meanwhile, organochlorine pesticides are known to interfere with inflammation responses in the host[47,48], and 4,4′-DDE was chosen due to its profound impact on *B.ovatus* metabolism (Supplementary Fig. 8c). The in vivo study comprised three mouse groups: named as ABX (only antibiotic-treated), Control (antibiotic-treated and 4,4′-DDE exposure), and BO (antibiotic-treated, *B.ovatus* transplantation and 4,4′-DDE exposure) groups (Fig. 5a, b). After 4,4′-DDE exposure in the Control and BO group, notable changes in microbial composition were observed (Fig. 5c), accompanied by insignificant body weight changes over 8 weeks (Fig. 5d) and detectable levels of 4,4′-DDE in mouse organs and tissues (Fig. 5e). Differential metabolomic profiles were evaluated between in vivo and in vitro studies (Supplementary Fig. 9 a-m). Next, a network analysis was performed to bridge the study outcomes between in vivo and in vitro, highlighting the dynamic interactions between microbiota and the host post pesticides exposure (Fig. 5f). The identified *B.ovatus*-associated metabolites following pesticides exposure (Fig. 3d) were also observed in tissues, including guanine in feces, cytidine-diphosphate (CDP)-ethanolamine and 5-aminovaleric acid in the lung (Fig. 5f). Other significantly altered microbial metabolites observed in vitro were also detected in multiple tissues—including feces, ileum, rectum, serum, lung, kidney, and testis—showing statistical significance between the Control and BO groups. As *B.ovatus* is part of the gut microbiota, its metabolic changes of its in vitro cultures are most directly linked to alterations in fecal metabolites. Consistently, we found that among the significantly altered metabolites, those overlapping between feces and *B.ovatus* cultures were most abundant. Nine metabolites significantly changed in both *B.ovatus* cultures and feces, including N-acylethanolamine (NAE) 18:1, NAE 5:0, pentadecanoic acid (FA 15:0), lysophosphatidylethanolamine (LPE) 15:0, xanthine, xanthosine, guanine, guanosine, and L-histidine. These metabolites play diverse roles, including cell signaling, membrane repair, purine metabolism, and immune response regulation[49,50]. Furthermore, the addition of *B.ovatus* in our mouse experiments influenced host metabolic processes, with a particular impact on lipid metabolism. Notably, 28 lipids from GLs, GPs, SPs, and STs (Fig. 5f) showed increased levels in the brain, while a significant decrease of lipids was observed in the rectum of BO-treated mice. Furthermore, the addition of *B.ovatus* in the BO group significantly increased straight- SCFAs[51] and secondary BAs[52] in the liver, brain and intestine of mice compared to the control group, which could act via the gastrointestinal tract to modulate the host immune system through gut-liver-brain axis[53–58] (Fig. 5g and Supplementary Fig. 9o–n). Subsequently, we observed the significantly lower levels of Toll-like receptor 4 (TLR4) and myeloid differentiation factor 88 (MyD88) in the BO group compared to the Control group, suggesting attenuated inflammation through TLR4/nuclear factor κB (NF-κB) inflammatory signaling pathway in the brain (Fig. 5g and Supplementary Fig. 9p). Additionally, this pathway regulated antioxidant activity and reduced malondialdehyde (MDA) levels (Supplementary Fig. 9q), a marker of lipid peroxidation. 4,4′-DDE exposure leads to significant alterations in propanoate metabolism (Fig. 3b) and bile acid metabolism (Fig. 3c) in vitro, and our mouse work suggested that these gut microbial metabolites also changed in vivo, which further modulate host immune system. Most SCFAs and BAs derived from *B.ovatus*, along with brain lipids (GLs, GPs, SPs, and STs), exhibited negative correlations with TLR4/ NF-κB pathway receptors (Supplementary Fig. 9r), reinforcing their potential anti-inflammatory role. The observed metabolic shifts link microbial activity with host physiology, emphasizing the relevance of these findings for understanding pesticide-induced systemic effects in the host that could be modulated by gut microbes.

Discussion

Previous studies have suggested that gut microbiota play a crucial role in pesticide breakdown and intricately mediate the impacts of pesticides on human health[59,60]. This relationship is partially characterized by alterations in gut microbial composition[61–64] as well as changes in host metabolites[65,66] following pesticide exposure. Recognizing that the gut microbial functions and metabolism may also be inadvertently impacted by pesticide, we aimed to assess the toxicity induced by pesticides on representative gut bacteria and its subsequent effects on host health via comprehensive metabolomics analyses. In our study, we found that pesticides disrupted the growth of individual gut bacteria, providing strong evidence for the previously observed gut microbiota imbalance following pesticide exposure[67–69]. Furthermore, the existence of bacteria capable of accumulating pesticides under pesticide exposure directly contributes to long-term pesticide residue or endocrine disruption in the host.

Pesticide exposure not only affects bacterial growth but also influences their metabolic activity. However, the links between gut microbial metabolites and host health remain poorly understood. We profiled 40 metabolic pathways and identified bacteria-specific metabolic changes in response to pesticides both in vitro and in vivo. This allowed us to characterize the hazards associated with gut microbiota-mediated pesticide exposure and its potential implications to host health. Notably, gut microbial derived bioactive lipids such as SCFAs, BAs, LPS, and the NAE family play critical roles in modulating inflammation, apoptosis, cardiometabolic disease, pain, obesity, and central nervous system disorders[70–76]. However, limited understanding of gut microbial lipids pathways and their connection to circulating lipids has hindered progress in uncovering how the human gut microbiota regulates host lipid homeostasis and physiological processes. In our study, we systemically analyzed lipid categories, classes, specific lipids, fatty acyl chain lengths, and saturation levels in gut bacteria following pesticide exposure. This work not only addresses the lack of microbial-lipid-specific datasets but also provide valuable insights into the role of gut microbial lipids in human health.

In summary, our current results, which includes bacteria-specific pesticide-metabolic profiles, offer a valuable resource for the comparative identification of biomarkers and the development of

https://doi.org/10.1038/s41467-025-59747-6

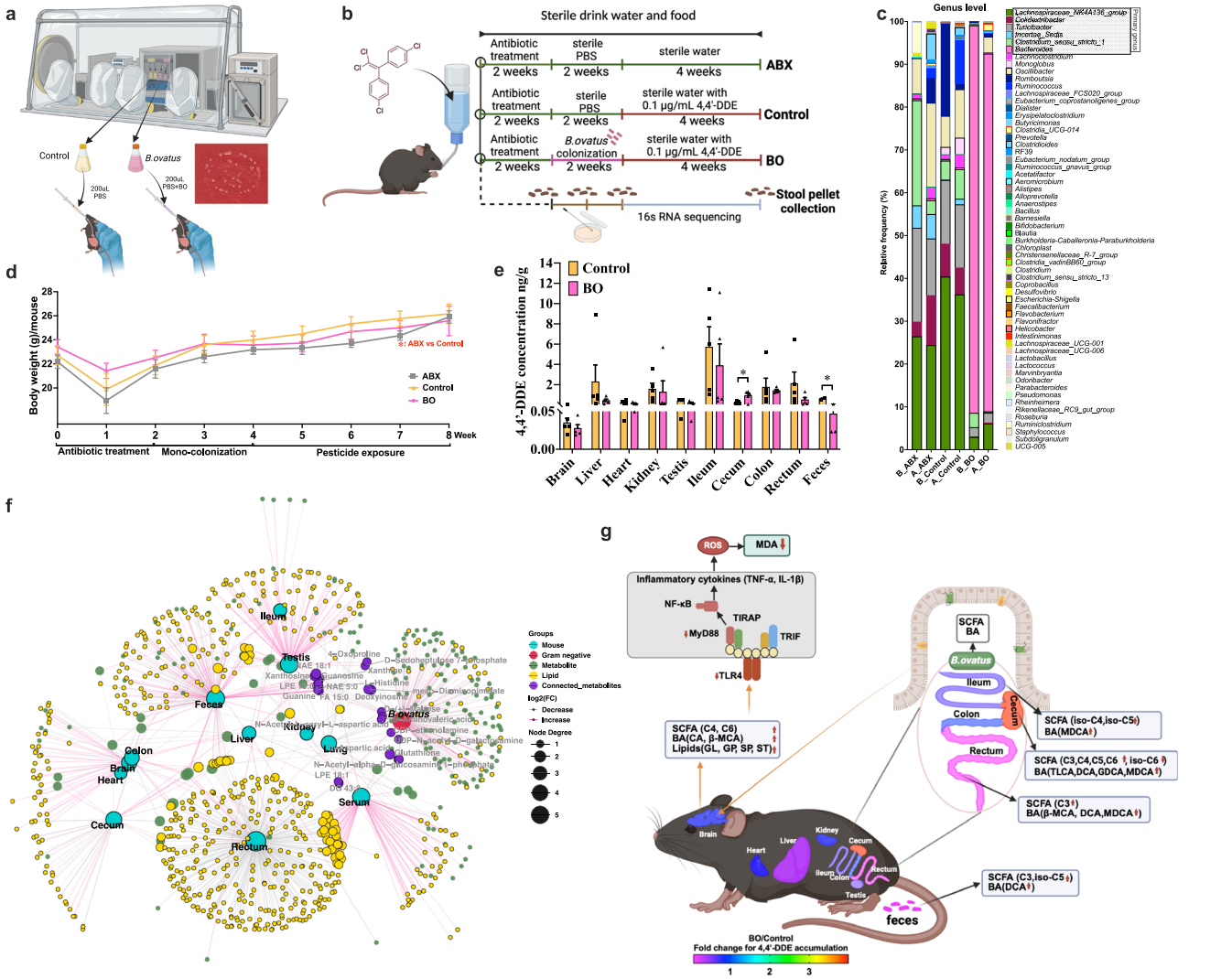

Fig. 5 | metabolic changes induced by 4,4′-DDE in C57BL/6 mice enriched with *B.ovatus*. **a** Cultivation of *B. ovatus* in anaerobic chamber and its inoculation into C57BL/6 mice via oral gavage. Created in BioRender. Gold, A. (2025) https://BioRender.com/l3kgcju. **b** Schematic representation of *B. ovatus* inoculation and 4,4′-DDE exposure in three groups of C57BL/6 mice. Created in BioRender. Gold, A. (2025) https://BioRender.com/2gnxlho. **c** Changes in gut microbiota composition before and after 4,4′-DDE exposure over four weeks in three groups. **d** The body weight of mice in the ABX, Control, and BO groups over 8 weeks ($n = 5$ biological replicates). **e** The 4,4′-DDE levels in mice tissues in the Control and BO group ($n = 5$ biological replicates), $p = 0.019$ in the cecum and $p < 0.001$ in feces. **f** Comprehensive network interaction analysis between gut microbiota-pesticide-metabolites using in vivo models. **g** Metabolic changes induced by 4,4′-DDE in C57BL/6 mice: targeted and untargeted analysis. Created in BioRender. Gold, A. (2025) https://BioRender.com/j071183. Data (d-e) is presented as mean ± SEM. p values were calculated by two-sided t test, and $p < 0.05$ represents statistically significant (**d**, **e**). ↑ indicates a significant decrease in BO vs Control (**g**); ↓ indicates a significant increase in BO vs Control (**g**); C3 propionic acid, C4 butyric acid, iso-C4 isobutyric acid, C5 valeric acid, iso-C5 isovaleric acid, C6 caproic acid, β-MCA β-muricholic acid, BAs bile acids, CA cholic acid, CDP cytidine-diphosphate, DCA deoxycholic acid, DG diacylglycerol, FC fold change, GL glycerolipid, GP glycerophospholipid, HCA hyocholic acid, GDCA glycodeoxycholic acid, LPE ether-linked lysppphosphatidylethanolamine, MDA malondialdehyde, MDCA murideoxycholic acid, MyD88 myeloid differentiation factor 88, NAE N-acyl ethanolamines, SCFAs short-chain fatty acids, SP sphingolipid, ST sterol lipid, TLCA taurolithocholic acid, TLR4 musculus toll-like receptor 4.

preventive strategies in understanding the interplay between gut bacteria and the host following pesticide exposure. Moreover, these data, along with the associated methodology, can serve as a direct reference or a readily deployable platform for enhancing the detection of microbiome-dependent metabolite perturbation in biological samples after pesticide exposure.

Our study aimed to enhance the fundamental understanding of pesticide exposure on gut bacteria, both in vitro and in vivo, in a generally healthy population. Given the complexity and diversity of the human gut microbiota, alongside the variability in environmental contaminants, we focused on a subset of gut bacteria and pesticides. This approach leaves many potential interactions unexamined. Currently, our research has concentrated solely on metabolomics and lipidomics outcomes. To gain a more comprehensive understanding, future research should integrate multi-omics approaches to identify functional genes, associated metabolites, and environmental contaminants. In the next phase of our study, we will explore gut microbiota-host co-metabolism across various health and disease states to elucidate the role of gut microbiota in human health under environmental contaminant exposure.

Methods

Growth conditions

The bacteria utilized in this study were obtained from the American Type Culture Collection (ATCC) and Coli Genetic Stock Center *(K12)* grown in Gifu anaerobic medium (GAM broth) in Coy anaerobic. The

bacterial strains employed in this research can be found in Supplementary Data 1. Anaerobic conditions were maintained using a nitrogen and hydrogen gas mixture, ensuring oxygen levels between 0 and 20 parts per million (ppm), alongside 2–3% hydrogen. The anaerobic state was monitored using the anaerobic monitor CAM-12. To eliminate oxygen and produce water molecules, two Stak-Pak systems equipped with palladium catalysts were employed. A vacuum airlock was utilized to minimize oxygen levels when transferring reagents or materials into and out of the glove box. Additionally, surfaces of equipment and materials were disinfected using 10% bleach and 75% alcohol. Glycerol stock of all bacterial strains was revived for plate streaking, and a single colony was transferred to GAM broth. Experimental cultures were initiated from the second passage culture following inoculation. We measured the growth curves of gut bacterial species to assess their distinct growth rates (Supplementary Fig. 1). Each species was cultured in 1 mL GAM medium at an initial optical density (OD_{590}) of 0.1 in a 5 mL Eppendorf tube. Growth was monitored in triplicate at 1, 5, 10, 24, and 48 h.

Pesticide dose-dependent growth inhibition

To evaluate the growth inhibition of individual bacteria species under anaerobic conditions, a concentration gradient (0.05 μg/mL, 0.1 μg/mL, 0.5 μg/mL, and 1 μg/mL) was employed for all pesticides. For most of tested pesticides, the 0.05–1 μg/mL concentrations were chosen to ensure it remained within the acceptable limits set by the pesticide maximum residue limits database from the US, EU and China, and represented a potential exposure concentration in the gastrointestinal tract (Supplementary Fig. 1a). Triplicate screenings for each bacterium-pesticide interaction were conducted within a 96-well deep plate. Prior to pesticide exposure, fresh Gifu anaerobic medium (GAM broth) was introduced into the anaerobic chamber the evening before. In order to assess dose-dependent growth inhibition caused by the pesticides, a 5 μL work solution of the pesticide, diluted with dimethyl sulfoxide (DMSO), or 5 μL of DMSO as a control, along with 1 mL of a second passage bacteria culture to achieve the OD 0.05 at 590 nm, were added to the 96-well deep plates under anaerobic conditions. The mixture was gently pipetted until thoroughly mixed and incubated at 37 °C for 3–5 h, depending on the growth rate of the bacteria. The growth of the bacteria was monitored by measuring the OD at 590 nm using a BioTek cytation 5. Statistical significance was assessed using a *T* test with a *p* value cutoff of 0.05.

Pesticide bioaccumulation detection and metabolism evaluation

Single bacteria strain from second passage culture were inoculated at a starting OD590 nm of 0.05 of 1 mL GAM culture containing 0.1 μg/mL pesticide in 96 well plates and incubated for 12 h while shaking at 37 °C under anaerobic condition. Plates were closed with lids.

To detect bioaccumulation, a combinatorial pooling strategy[77] was employed to allocate 18 pesticides into 8 pools, ensuring that each pesticide was represented in quadruplicate (Supplementary Fig. 2a). After 12 h, the 96-well plates containing the bacteria culture were sealed and removed from the anaerobic chamber for storage at −80 °C until analysis. To determine the pesticide concentration in the bacterial strains using GC-QQQ MS, the 96-well plate needed to be thawed at 4 °C for 15 h, followed by centrifugation at 3122 × g for 20 min. The supernatant was discarded, and the pellet was washed three times with 1 mL of PBS (pH 7.4). A pesticide extraction solution was prepared using acetonitrile and 0.050 μg/mL of chlorpyriphos-methyl as an internal standard. After adding 300 μL of the extraction solution and vortexing for 1 min, 300 μL of the mixture was transferred into a 2 mL Eppendorf tube containing 0.5 g of NaCl. The same steps were repeated by adding 300 μL of the extraction solution back into the 96-well plate. Finally, the 600 μL of the extraction solution was combined and vortexed for 3 min. After centrifugation at 10,000 r/min for 3 min, all the supernatant was transferred into a 2 mL dSPE tube with two 3 mm glass beads for purification. The sample was homogenized for 15 s using a Beadbeater (MiniBeater-16, Model 507) for a total of three cycles, followed by centrifugation at 10,000 r/min for 3 min. The resulting supernatant was transferred into 2 mL glass vials with glass inserts for GC-QQQ MS analysis.

To assess metabolism, 18 individual pesticides were added in quadruplicate to a 96-well plate, along with 1 mL of a single bacteria culture at a starting OD590nm of 0.05. Two plates with the same pesticide combinations were prepared for subsequent metabolomics and lipidomics analyses. After 12 h, the 96-well plates were covered with sealing films and removed from the anaerobic chamber, then stored at −80 °C until analysis. Prior to extraction, the frozen 96-well plates were thawed at 4 °C for 15 h and subsequently centrifuged at 3122 × *g* for 20 min. The supernatant was discarded, and the pellet was washed three times with 0.5 mL of PBS (pH 7.4). For metabolomics extraction, an extraction solution containing methanol and 200 μg/mL of 13 C,15N-amino acids as an internal standard were prepared. After adding 300 μL of the extraction solution to the 96-well plates, the samples were vortexed for 3 min and kept at −20 °C for 20 min. Following centrifugation at 3122 × *g* and 4 °C for 20 min, the supernatant was collected in a 2 mL glass vial with an insert for UPLC-QE orbitrap analysis. As for lipidomics extraction, the extraction solution was a mixture of 2-propanol and 0.275 μg/mL of 13C-labeled lipids as an internal standard. After adding 290 μL of the lipid extraction solution, the samples were vortexed for 2 minmin and ultrasonicated in ice water for 20 min, followed by standing at 4 °C for 30 min. After centrifugation at 3122 × *g* and 4 °C for 20 min, the supernatant was collected in a 2 mL glass vial with an insert for UPLC-QE orbitrap MS analysis.

Mouse experiment

All animal experiments conducted in this study were carried out following the approved protocols by the Ohio State University Institutional Laboratory Animal Care and Use Committee. Male C57BL/6 mice ($n = 24$) aged 7 weeks and obtained from Jackson Lab were housed in a controlled environment at 25 °C with a 12-h light-dark cycle. Following a one-week acclimation period, the mice were randomly assigned to three groups, with 8 mice per group. Mice received sterile chow (7012) and water ad libitum throughout the study. The four groups were designated as ABX, Control, and BO, corresponding to specific periods as outlined below.

Period 1: a pseudo germ-free mouse model was established by treating all groups of mice with broad-spectrum antibiotics. At 8 and 9 weeks of age, the mice received a continuous administration of ampicillin (1 g/L), neomycin sulfate (1 g/L), and metronidazole (1 g/L) obtained from Sigma-Aldrich Co. Ltd, USA, which were dissolved in their drinking water. This antibiotic treatment lasted for 14 consecutive days. The drinking solution was replaced and documented every 2 days, while sterile food was refreshed and recorded on a weekly basis.

Period 2: In the mono-colonization experiments, B. ovatus was cultured in an anaerobic chamber and their identities were confirmed through phenotype verification using GAM plate streaking and PCR primers. For B. ovatus, the primers used were as follows: Forward: 5′–3′ TGCAAACTRAAGATGGC and Reverse: 5′–3′ CAAACTAATGGAACGCATC. After culturing for 24 h, a 10 mL saturated bacterial culture was centrifuged and washed three times with PBS. The bacterial pellets were then resuspended in 10 × 1 mL sterile PBS in 2 mL sterile Eppendorf tubes. In the BO group, mice were colonized with *B. ovatus* ATCC8483 (approximately 8 × 10^6 colony-forming units (CFU)) obtained from the saturated cultures. This colonization process involved orally administering 200 μL of the respective cultures through gavage. On the other hand, mice in the ABX and Control

groups were only orally gavaged with 200 µL of PBS. Fecal samples were collected both before and after mono-colonization for phenotype verification. The sterile water was replaced and documented every 2 days, and sterile food was refreshed and recorded on a weekly basis.

Period 3: Regarding pesticide exposure, once successful mono-colonization was achieved, the mice from the Control, and BO groups were subjected to a 4-week exposure to 0.1 µg/mL of 4,4′-DDE in their drinking water. Meanwhile, the mice in the ABX group received sterile water without pesticide. The drinking water was replaced and documented every 2 days, and sterile food was refreshed and recorded on a weekly basis. Prior to and after mono-colonization, 16S amplicon sequencing was performed on the V4 region (515 F, 806 R) of microbial populations found in individual mice's feces. Following the completion of the above-mentioned three periods, the mice ($n = 5$) were euthanized using CO2. Thirteen different sample types (serum, brain, liver, lung, heart, spleen, kidney, testis, ileum, cecum, colon, rectum, and feces) were collected and weighed from each mouse. All samples were divided into five replicates and stored at −80 °C until further analysis. In the mouse experiments, a single biological replicate represents a specific sample type, such as serum, obtained from an individual mouse. This means that each biological replicate is derived from a different mouse. Prior to euthanization, feces were collected, and blood samples were taken from the heart and centrifuged to obtain serum for subsequent analysis. The contents from the ileum, cecum, colon, and rectum were thoroughly removed.

Mouse samples preparation for pesticide analysis

To begin the extraction process, take 50 µl of serum, 100–300 mg of feces, or 10–400 mg of tissues and transfer them into a 2 mL dSPE tube containing 2 beads for pesticide extraction. Add 800–1000 µl of acetonitrile to the tube, adjusting the volume based on the mass or volume of the samples. Vortex the mixture using a beadbeater for 15 s (or 60 s for samples from the ileum, cecum, colon, or rectum), repeating this step three times. Subsequently, centrifuge the tube at room temperature and 13,709 × g for 10 min. Carefully transfer the resulting supernatant, which should be around 600–800 µL, into 2 mL Eppendorf tubes for further processing using a speedvac.

To redissolve the sample, add 100 µl of isooctane and the internal standard (chlorphriphos-methyl at a concentration of 0.05 µg/mL). Centrifuge the mixture once again at room temperature and 13,709 × g for 10 min. Transfer the supernatant into a 2 mL glass vial with a glass insert for subsequent analysis. Finally, subject the samples to GC-QQQ MS to detect 4,4′-DDE and its metabolites 4,4′-DDD.

Mouse samples preparation for SCFAs, BAs, and metabolomics analysis

The process involved weighing 50 µL of serum, 100–200 mg of feces, and 10–100 mg of tissue samples into 2 mL polypropylene microvials. Two glass beads and 300-500 µL of methanol with 200 µg/mL of 13 C,15N-amino acids were added to facilitate homogenization using a beadbeater for 15 s (repeated three times with 60-second intervals). The mixture was then sonicated in ice water for 30 min and left at −20 °C for 20 min. Following centrifugation at 18,659 × g and 4 °C for 20 min, 180 µL of supernatant was transferred into a 2 mL glass vial with an insert for bile acids (BAs) and metabolomics analysis. For SCFAs (short-chain fatty acids) derivatization, 40 µL of supernatant from serum, feces, liver, brain, ileum, cecum, colon, and rectum was transferred into a 2 mL Eppendorf tube. This step followed our previously published method[78]. To summarize, either a 40 µL standard solution or a 40 µL supernatant was thoroughly mixed with 20 µL of a 200 mM 3NPH·HCl solution and 20 µL of a 120 mM EDC·HCl-6% pyridine solution. The samples were vortexed for 2 min and then incubated in a 40 °C water bath for 30 min. Following that, the samples were cooled on ice for 1 min. Depending on the sample, either 420 µL or 920 µL of a 10% acetonitrile solution was used to dilute the derivatized samples before conducting UPLC-QE Orbitrap MS analysis. Due to the high concentration of acetic acid in the samples, all diluted samples still required a further dilution of 20 times before reanalysis by UPLC-QE Orbitrap MS.

Mouse samples preparation for lipidomics analysis

To begin, approximately 20 mg samples of kidney, lung, heart, testis, ileum, cecum, colon, rectum, and feces, along with 20 µL of serum, were weighed into 2 mL microvials. A lipid extraction solution consisting of 200 µL of 2-propanol with 0.275 µg/mL 13C-labeled lipids was added to the microvials. For brain samples weighing 10–100 mg and liver samples weighing 75–350 mg, 300 µL and 1 mL of the lipid extraction solution, respectively, were added to facilitate sample extraction. In all vials, 2 glass beads were included for homogenization using a Beadbeater, either for 15 s or 60 s, repeated three times. The homogenized samples were then subjected to ultrasonication in ice water for 20 min and left to stand overnight at −20 °C. The following day, the samples were centrifuged at 18,659 × g and 4 °C for 10 min, and the resulting supernatant was collected into a 2 mL glass vial with an insert for UPLC-QE Orbitrap MS analysis.

GC-QQQ MS methods

Data acquisition was performed using an Agilent 8890 GC system coupled with a 7010 Triple Quadrupole mass spectrometer (GC-QQQ MS), which was equipped with a Gerstel autosampler. Data analysis was conducted using Agilent MassHunter Quantitative analysis software. For separation, a J&W DB-5MS column with a 95% dimethyl/5% diphenyl polysiloxane composition, measuring 30 meters in length, 0.25 millimeters in internal diameter, and coated with a 0.25-micrometer film, was used. Additionally, a 10-meter empty DuraGuard guard column was employed. Samples of 1 µL were injected using an Agilent ultra-inert inlet liner with a 4 mm ID, utilizing a splitless, single taper, wool configuration. The inlet temperature was set to 250 °C with splitless mode, and the gas saver was set to 20 mL/min after 3 min. Helium gas was used as the carrier gas with a flow rate of 1.005 mL/min. Nitrogen served as the collision gas at a rate of 1.5 mL/min, while helium was utilized as the quenching gas at 4 mL/min. The initial oven temperature was 60 °C for 1 min, followed by an increase of 40 °C/min to 170 °C, and then an increase of 10 °C/min to 310 °C, which was held for 10 min. The total run time was 27.75 min. For the post-run period, the temperature was set at 320 °C, and the flow rate was maintained at 1.2 mL/min for 5 min. The MSD transfer line temperature was 280 °C, the ion source temperature was 280 °C, the quadrupole temperature was 150 °C, and a gain factor of 1 was applied. In dMRM (dynamic multiple reaction monitoring) mode, 18 pesticides, each with at least two pairs of precursor and product ions, were selected for both qualitative and quantitative analysis. The mass resolution of both MS1 and MS2 was set to wide. A targeted pesticide method was established and validated. As an initial step in evaluating the analytical performance, the pesticide method was verified to exhibit good linearity and recovery, as demonstrated in Supplementary Fig. 2c. To determine the final pesticide concentrations in samples obtained from in vivo or in vitro experiments, a 50 ng/mL Chlorpyriphos-methyl internal standard was utilized for calculation purposes.

UPLC-QE Orbitrap MS methods

This study utilized a Thermo Vanquish UPLC system coupled with a Q-Exactive Orbitrap mass spectrometer (UPLC-QE Orbitrap MS) equipped with a heated electrospray ionization (HESI) probe from Thermo Fisher in California, USA. For metabolomics analysis, a Waters Xbridge BEH Amide 2.5 µm 2.1 × 150 mm column was employed to separate polar metabolites in both negative and positive ionization modes, with separate injections for each mode. Mobile phase A consisted of a mixture of acetonitrile and water (10/90, v/v), containing

5 mM ammonium acetate and 0.1% acetic acid. Mobile phase B comprised a mixture of acetonitrile and water (90/10, v/v), also containing 5 mM ammonium acetate and 0.1% acetic acid. A linear gradient elution program was employed, starting with 70% B from 0 to 0.1 min, decreasing to 30% B from 0.1 to 5 min, holding for 4 min, and then returning to 70% B by 2 min and holding for 9 min. The total run time was 20 min, with a flow rate of 0.30 mL/min and a column temperature of 40 °C. The data collection resolution for full scan analysis was set to 70,000 within the m/z range of 60–900. The automatic gain control (AGC) target was 3e6, and the maximum ion trap (IT) time was 200 ms.

For bile acids (BAs) analysis, a Phenomenex Kinetix C18 column (2.6 μm, 150 mm × 4.6 mm ID) was used for separation in negative ionization mode, following our previously reported method[79]. The mobile phase A consisted of a methanol:acetonitrile:water mixture (1:1:3, v/v/v) with 1 mM ammonium acetate and 0.1% acetic acid, while mobile phase B consisted of a methanol:acetonitrile:2-propanol mixture (4.5:4.5:1, v/v/v) with 0.1% acetic acid. Gradient elution was applied, and MS1 and MS2 data were collected using the PRM mode and t-SIM mode.

For SCFAs analysis, CSH C18 1.7μm 2.1 × 100mm column (Waters Corp, Milford, MA, USA) was applied for SCFAs separation in negative ionization mode[78]. The mobile phase A consisted of water with 0.1% formic acid, and mobile phase B comprised acetonitrile with 0.1% formic acid. MS1 and MS2 data were acquired using the PRM mode and t-SIM mode.

For lipidomic analysis, an Acquity UPLC CSH C18 1.7 μm 2.1 × 100 mm column (Waters Corp, Milford, MA, USA) was utilized for separation of lipid metabolites in both negative and positive ionization modes, following our previously reported method[80]. Mobile phase A consisted of a mixture of acetonitrile and water (60/40, v/v), containing 10 mM ammonium acetate and 0.1% formic acid. Mobile phase B comprised a mixture of acetonitrile and 2-propanol (10/90, v/v), also containing 10 mM ammonium acetate and 0.1% formic acid. Full scan/ddMS^2 mode was used to acquire MS1 and MS2 information.

qRT-PCR analysis

Liver and brain samples were homogenized in TRIzol reagent at a ratio of 1 mL per 50-100 mg of tissue. Following homogenization, the mixtures were incubated at room temperature for 5 min. Next, 100 μL of BCP was added to the mixture and incubated again at room temperature for 5 min. The samples were then centrifuged at 18659 × g and 4 °C for 8 min, and the resulting supernatant was carefully transferred to a fresh 1.5 mL microtube. To precipitate the RNA, 250 μL of a high salt precipitation solution and 250 μL of 2-propanol were added and incubated at room temperature for 10 min. After centrifugation at 18,659 × *g* and 4 °C for 5 min, the supernatant was aspirated off, and the RNA pellets were air-dried at room temperature for approximately 5–10 min. Finally, 50–200 μL of DEPC water was used to dissolve the RNA. After quantifying the RNA, the concentration was adjusted to 200 ng/μL for cDNA synthesis using the iScript cDNA synthesis kit from Bio-Rad. The synthesized cDNA was stored at −20 °C for qRT-PCR analysis. 10 primer pairs were compiled and listed in Supplementary Data 6.

16s RNA sequencing

Briefly, PCR amplicon libraries targeting the 16S rRNA encoding gene present in metagenomic DNA are produced using a barcoded primer set adapted for the Illumina HiSeq2000 and MiSeq. Specifically, the V4 region of the 16S rRNA gene (515F-806R) is PCR amplified with region-specific primers that include sequencer adapter sequences used in the Illumina flowcell. Each 25 μL PCR reaction contains 9.5 μL of MO BIO PCR Water (Certified DNA-Free), 12.5 μL of QuantaBio's AccuStart II PCR ToughMix (2x concentration, 1x final), 1 μL Golay barcode tagged Forward Primer (5 μM concentration, 200 pM final), 1 μL Reverse Primer (5 μM concentration, 200 pM final), and 1 μL of template DNA. The conditions for PCR are as follows: 94 °C for 3 min to denature the DNA, with 35 cycles at 94 °C for 45 s, 50 °C for 60 s, and 72 °C for 90 s; with a final extension of 10 min at 72 °C to ensure complete amplification. Amplicons are then quantified using PicoGreen (Invitrogen) and a plate reader (InfiniteÒ 200 PRO, Tecan). Once quantified, volumes of each of the products are pooled into a single tube so that each amplicon is represented in equimolar amounts. This pool is then cleaned up using AMPure XP Beads (Beckman Coulter), and then quantified using a fluorometer (Qubit, Invitrogen). After quantification, the molarity of the pool is determined and diluted down to 2 nM, denatured, and then diluted to a final concentration of 6.75 pM with a 10% PhiX spike for sequencing on the Illumina MiSeq. Amplicons are sequenced on a 151 bp x 12 bp x 151 bp MiSeq run using customized sequencing primers and procedures. QIIME 2 was used for 16S data analysis.

Data analysis

Masshunter quantitative analysis. Data analysis of GC-QQQ MS was conducted using Agilent MassHunter Quatitative Analysis version 10.2 software (Agilent Technologies). A new analysis method was generated based on the acquired MRM data. The software automatically populated the precise precursor and product ions as well as the retention time in certain sections of the data analysis method. The quantitative ion pairs and retention time for both in vitro (15 pesticides and 3 metabolites) and in vivo (4,4′-DDE and 4,4′-DDD) samples were manually verified and adjusted if necessary. Subsequently, the method was saved and utilized for batch quantification of all samples.

Compound discover analysis

For the metabolomics analysis, the Compound Discover software (version 3.3, Thermo Fisher Scientific) was employed to process and analyze the '.raw' data files obtained from the UPLC-QE Orbitrap MS. To initiate the data processing task, a new study was created, and a customized non-targeted metabolomics workflow was employed for data processing. The '.raw' data files were added to the project and categorized into three predefined groups: Blank, Samples, and Identification only. The identification of compounds was performed using mzCloud (ddMS2), ChemSpider (formula or exact mass), and an in-house database containing m/z values of 171 standards and 20 13C15N amino acids. The workflow included retention time correction, feature detection, and chromatogram alignment. The parameters used were as follows: polarity (positive $[M+H]^+$ or negative $[M-H]^-$) determined by the raw data, maximum shift of 0.2 min, mass tolerance of 5 ppm, and a minimal peak intensity of 1×10^4. After data processing, a characteristic table was generated based on the m/z and retention time of each molecule, which provided the peak areas of each compound across all samples. Subsequently, the data was normalized and exported in.csv format. Quality control (QC) samples were utilized to calculate the coefficient of variation (CV) for each compound, and compounds with CV values less than 20% were selected for further statistical analysis.

MS-DIAL analysis

The lipidomics analysis involved the utilization of the MS-DIAL software (version) to analyze all in vitro and in vivo data acquired from the UPLC-QE Orbitrap MS. The raw data acquisition was performed using Xcalibur 4.0 software (Thermo Fisher Scientific, USA). Subsequently, the raw data from the DDA and DIA experiments were converted from the vendor-specific file format (.raw) to the Analysis Base File format (.abf) using the freely available Reifycs ABF converter (https://www.reifycs.com/AbfConverter/).

After conversion, the MS-DIAL software (version 4.24) was employed for various data processing tasks, including feature

detection, spectral deconvolution, peak identification, and alignment between samples. Quality control samples (QC) from each bacteria strain or mice samples were used for peak alignment. During the analysis, specific adducts were selected based on the ionization mode. In positive ionization mode, adducts such as $[M+H]^+$, $[M+NH4]^+$, $[M+Na]^+$, $[M+ACN+H]^+$, $[M+H\text{-}H2O]^+$, $[M+H\text{-}2H2O]^+$, $[2M+H]^+$, and $[M+2H]^{2+}$ were chosen, while in negative ionization mode, adducts including $[M\text{-}H]^-$, [M-H2O-H]-, $[M+Na\text{-}2H]^{2-}$, $[M+FA\text{-}H]^-$, $[M+Hac\text{-}H]^-$, $[2M\text{-}H]^-$, and $[M\text{-}2H]^{2-}$ were selected. The lipid database settings were kept as default for both positive and negative ion modes.

Chemical assignment of molecular features in the samples was performed by comparing the recorded retention time (RT) and m/z information to the reference library constructed from authentic standards. Tolerance windows of 0.05 min for RT and 0.01 Da for m/z were set. To filter the results, a minimal peak count filter of 5000 or a signal-to-noise ratio (S/N) filter of 10 was applied to all samples. The MS-DIAL analysis generated a comprehensive list of metabolite names, m/z values, RT values, formulas, ontologies, INCHIKEYs, SMILES representations, S/N ratios, and peak areas for high confidence annotations, as well as all unknown molecular features for both positive and negative polarity modes. Specific metabolite features were excluded from the list under the following conditions: (1) if they were detected only in the blank controls, (2) if the coefficient of variation (CV) in the QC samples was higher than 20%, (3) if the annotated compounds were identified in both positive and negative polarity modes and had lower peak areas or S/N ratios, or higher CV values, and (4) if the molecular features were unknown, they were also removed for further analysis.

Statistics and reproducibility

The results were presented as mean ± SE, statistical analysis and data visualization were conducted using GraphPad Prism 9 software, OriginLab 2020, Biorender, and R Studio. For normally distributed data, a two-tailed unpaired Student's *t* test was performed. To control the false discovery rate (FDR), the *p* values were adjusted using the Benjamini-Hochberg (BH) method. For the in vitro study, statistical significance was defined as an adjusted *p* value of <0.05 after multiple testing correction to account for potential false discoveries. For the in vivo study, a less stringent criterion of *p* value < 0.05 (without adjustment) was used to identify significant changes, acknowledging the difference in sensitivity and variability between in vitro and in vivo conditions. This approach ensures meaningful interpretation while reflecting the biological context of each study type. TidyMass software was utilized for the analysis of metabolomics and lipidomics data[81]. To conduct data analysis, three data frames were created: expression_data, sample_info, and variable_info. These data frames were utilized by the libraries (massdataset, massstat, metpath) to generate various plots and related statistical data-resources. Each experimental group was compared with its respective control group. All significantly altered metabolites (FDR adjusted $p < 0.05$ and $|Log2(FC)| > 1$) were visualized as heatmaps in Supplementary Figs. 3a, 5a. To enhance the clarity of heatmap visualization while preserving meaningful biological patterns, we applied a targeted filtering strategy to the matrix of statistically significant compounds. In this dataset, missing values do not indicate technical errors but rather reflect compounds that were either not significantly altered or not detected in certain samples. To ensure that each visualized metabolite and sample contained a sufficient level of informative signal, we first retained only those compounds (rows) that showed significant values in more than 10 samples. Subsequently, we filtered the matrix to retain only those samples (columns) that contained significant values for more than 10 compounds. This approach allowed us to focus the heatmap on the most informative and interpretable portion of the data (Supplementary Fig. 3b and Supplementary Fig. 5b).

Given the complex composition of lipids, including different functional groups, fatty acyl chains, and double bonds, these characteristics were also summarized and depicted. Finally, all statistical data-resources were further summarized and visualized by Prism and OriginLab. We performed network analysis to visualize the relationships among nodes categorized into predefined groups based on their biological or chemical properties. The analysis was conducted using igraph and ggraph libraries in R. Data for edges and nodes were loaded from CSV files, ensuring the presence of essential columns (from, to, and connection_strength for edges; name and group for nodes). Node groupings were validated against a set of predefined categories (e.g., "Gram positive," "Gram negative," and "Pesticide") and visualized using a custom color scheme to highlight group distinctions. Graph esthetics, including node size (calculated as the logarithm of node degree) and edge transparency (scaled by connection strength), were defined to enhance interpretability. Nodes representing "Gram positive" or "Gram negative" groups with high connectivity (degree > 3) were labeled to emphasize significant connections. A Kamada-Kawai layout was employed to position nodes, and edge directions were omitted to reflect undirected relationships. The final network plot was created with comprehensive legends for node groups, edge colors (indicating increased or decreased connection strength), and node sizes.

Data availability

The raw metabolomics data for the in vitro and in vivo experiments can be accessed publicly on MassIVE under study number MSV000095526, MSV000095539, and MSV00095671. 16S rRNA sequencing data have been deposited in figshare and are available at: https://doi.org/10.6084/m9.figshare.28837370. All supplementary data generated in this study are provided in Supplementary Data 1–6. The source data underlying all figures are provided as a Source Data file. Source data are provided with this paper.

Code availability

We developed custom R code to facilitate the processing and visualization of the UPLC-QE Orbitrap MS data obtained from the in vitro and in vivo experiments. All original code has been uploaded into https://data.mendeley.com/datasets/9f5xzypspc/1 (https://doi.org/10.17632/9f5xzypspc.1) for peer review. This code provides a comprehensive toolkit for data analysis and facilitates the exploration of various aspects of the metabolomics and lipidomics datasets.

References

1. Schulz, R., Bub, S., Petschick, L. L., Stehle, S. & Wolfram, J. Applied pesticide toxicity shifts toward plants and invertebrates, even in GM crops. *Science* **372**, 81–84 (2021).
2. Hallmann, C. A., Foppen, R. P., Van Turnhout, C. A., De Kroon, H. & Jongejans, E. Declines in insectivorous birds are associated with high neonicotinoid concentrations. *Nature* **511**, 341–343 (2014).
3. Nicholson, C. C. et al. Pesticide use negatively affects bumble bees across European landscapes. *Nature* **628**, 355–358 (2024).
4. Landrigan, P. J. et al. The Lancet Commission on pollution and health. *Lancet* **391**, 462–512 (2018).
5. Kniss, A. R. Long-term trends in the intensity and relative toxicity of herbicide use. *Nat. Commun.* **8**, 1–7 (2017).
6. Gevao, B., Semple, K. T. & Jones, K. C. Bound pesticide residues in soils: a review. *Environ. Pollut.* **108**, 3–14 (2000).
7. Maggi, F., Tang, F. H. & Tubiello, F. N. Agricultural pesticide land budget and river discharge to oceans. *Nature* **620**, 1013–1017 (2023).
8. Kruse-Plaß, M., Hofmann, F., Wosniok, W., Schlechtriemen, U. & Kohlschütter, N. Pesticides and pesticide-related products in ambient air in Germany. *Environ. Sci. Eur.* **33**, 1–21 (2021).

9. Hamilton, D. et al. Pesticide residues in food—acute dietary exposure. *Pest Manag. Sci. Former. Pestic. Sci.* **60**, 311–339 (2004).
10. Syafrudin, M. et al. Pesticides in drinking water—a review. *Int. J. Environ. Res. Public health* **18**, 468 (2021).
11. Cancino, J. et al. Occupational exposure to pesticides and symptoms of depression in agricultural workers. A systematic review. *Environ. Res.* **231**, 116190 (2023).
12. Hold, G. L. Gastrointestinal microbiota and colon cancer. *Digest. Dis.* **34**, 244–250 (2016).
13. Gasaly, N., De Vos, P. & Hermoso, M. A. Impact of bacterial metabolites on gut barrier function and host immunity: a focus on bacterial metabolism and its relevance for intestinal inflammation. *Front. Immunol.* **12**, 658354 (2021).
14. Hugon, P. et al. A comprehensive repertoire of prokaryotic species identified in human beings. *Lancet Infect. Dis.* **15**, 1211–1219 (2015).
15. Cerdó, T. et al. Role of microbiota function during early life on child's neurodevelopment. *Trends Food Sci. Technol.* **57**, 273–288 (2016).
16. Wang, Y. & Kasper, L. H. The role of microbiome in central nervous system disorders. *Brain, Behav., Immun.* **38**, 1–12 (2014).
17. Oriá, R. B. et al. Early-life enteric infections: relation between chronic systemic inflammation and poor cognition in children. *Nutr. Rev.* **74**, 374–386 (2016).
18. Lynch, S. V. & Pedersen, O. The human intestinal microbiome in health and disease. *N. Engl. J. Med.* **375**, 2369–2379 (2016).
19. Gopalakrishnan, V., Helmink, B. A., Spencer, C. N., Reuben, A. & Wargo, J. A. The influence of the gut microbiome on cancer, immunity, and cancer immunotherapy. *Cancer cell* **33**, 570–580 (2018).
20. Barcik, W., Boutin, R. C., Sokolowska, M. & Finlay, B. B. The role of lung and gut microbiota in the pathology of asthma. *Immunity* **52**, 241–255 (2020).
21. DiBaise, J. K. et al. In *Mayo clinic proceedings*. 460–469 (Elsevier).
22. Ferreiro, A. L. et al. Gut microbiome composition may be an indicator of preclinical Alzheimer's disease. *Sci. Transl. Med.* **15**, eabo2984 (2023).
23. Abdollahi, M., Ranjbar, A., Shadnia, S., Nikfar, S. & Rezaie, A. Pesticides and oxidative stress: a review. *Med. Sci. Monit.* **10**, 141–147 (2004).
24. Sule, R. O., Condon, L. & Gomes, A. V. A common feature of pesticides: oxidative stress—the role of oxidative stress in pesticide-induced toxicity. *Oxid. Med. Cell. Longev.* **2022**, 5563759 (2022).
25. Bourzac, K. People who are changing the environment one community at a time. *Nature* **621**, 35–37 (2023).
26. Mostafalou, S. & Abdollahi, M. Pesticides and human chronic diseases: Evidences, mechanisms, and perspectives. *Toxicol. Appl. Pharmacol.* **268**, 157–177 (2013).
27. Chang, X. et al. Impact of chronic exposure to trichlorfon on intestinal barrier, oxidative stress, inflammatory response and intestinal microbiome in common carp (Cyprinus carpio L.). *Environ. Pollut.* **259**, 113846 (2020).
28. Rouzé, R., Moné, A., Delbac, F., Belzunces, L. & Blot, N. The honeybee gut microbiota is altered after chronic exposure to different families of insecticides and infection by Nosema ceranae. *Microbes Environ.* **34**, 226–233 (2019).
29. Smith, L. et al. Perinatal exposure to a dietary pesticide cocktail does not increase susceptibility to high-fat diet-induced metabolic perturbations at adulthood but modifies urinary and fecal metabolic fingerprints in C57Bl6/J mice. *Environ. Int.* **144**, 106010 (2020).
30. Arumugam, M. et al. Enterotypes of the human gut microbiome. *nature* **473**, 174–180 (2011).
31. Kim, J. et al. 4, 4′-Dichlorodiphenyltrichloroethane (DDT) and 4, 4′-dichlorodiphenyldichloroethylene (DDE) promote adipogenesis in 3T3-L1 adipocyte cell culture. *Pestic. Biochem. Physiol.* **131**, 40–45 (2016).
32. Takeuchi, T. et al. Gut microbial carbohydrate metabolism contributes to insulin resistance. *Nature* **621**, 389–395 (2023).
33. Masse, K. E. & Lu, V. B. Short-chain fatty acids, secondary bile acids and indoles: Gut microbial metabolites with effects on enteroendocrine cell function and their potential as therapies for metabolic disease. *Front. Endocrinol.* **14**, 1169624 (2023).
34. Brown, J. M. & Hazen, S. L. The gut microbial endocrine organ: bacterially derived signals driving cardiometabolic diseases. *Annu. Rev. Med.* **66**, 343–359 (2015).
35. Brown, E. M., Clardy, J. & Xavier, R. J. Gut microbiome lipid metabolism and its impact on host physiology. *Cell Host Microbe* **31**, 173–186 (2023).
36. Řezanka, T. & Sigler, K. Odd-numbered very-long-chain fatty acids from the microbial, animal and plant kingdoms. *Prog. Lipid Res.* **48**, 206–238 (2009).
37. Venn-Watson, S. & Schork, N. J. Pentadecanoic acid (C15: 0), an essential fatty acid, shares clinically relevant cell-based activities with leading longevity-enhancing compounds. *Nutrients* **15**, 4607 (2023).
38. Pfeuffer, M. & Jaudszus, A. Pentadecanoic and heptadecanoic acids: Multifaceted odd-chain fatty acids. *Adv. Nutr.* **7**, 730–734 (2016).
39. Wang, J. et al. Caprylic acid and nonanoic acid upregulate endogenous host defense peptides to enhance intestinal epithelial immunological barrier function via histone deacetylase inhibition. *Int. Immunopharmacol.* **65**, 303–311 (2018).
40. Vinogradov, E., Perry, M. B. & Conlan, J. W. Structural analysis of Francisella tularensis lipopolysaccharide. *Eur. J. Biochem.* **269**, 6112–6118 (2002).
41. Phillips, N. J., Schilling, B., McLendon, M. K., Apicella, M. A. & Gibson, B. W. Novel modification of lipid A of Francisella tularensis. *Infect. Immun.* **72**, 5340–5348 (2004).
42. Wang, X. et al. Structure and biosynthesis of free lipid A molecules that replace lipopolysaccharide in Francisella tularensis subsp. novicida. *Biochemistry* **45**, 14427–14440 (2006).
43. Brown, G. C. The endotoxin hypothesis of neurodegeneration. *J. Neuroinflamm.* **16**, 180 (2019).
44. Giordano, N. P., Cian, M. B. & Dalebroux, Z. D. Outer membrane lipid secretion and the innate immune response to gram-negative bacteria. *Infect. Immunity* **88**, https://doi.org/10.1128/iai.00920-00919 (2020).
45. Satapati, S. et al. Mitochondrial metabolism mediates oxidative stress and inflammation in fatty liver. *J. Clin. Investig.* **125**, 4447–4462 (2015).
46. Zhang, Y.-M. & Rock, C. O. Membrane lipid homeostasis in bacteria. *Nat. Rev. Microbiol.* **6**, 222–233 (2008).
47. Wang, X. et al. Associations of dietary exposure to organochlorine pesticides from plant-origin foods with lipid metabolism and inflammation in women: a multiple follow-up study in North China. *Bull. Environ. Contam. Toxicol.* **107**, 289–295 (2021).
48. Peinado, F., Artacho-Cordón, F., Barrios-Rodríguez, R. & Arrebola, J. Influence of polychlorinated biphenyls and organochlorine pesticides on the inflammatory milieu. A systematic review of in vitro, in vivo and epidemiological studies. *Environ. Res.* **186**, 109561 (2020).
49. Tsuboi, K., Uyama, T., Okamoto, Y. & Ueda, N. Endocannabinoids and related N-acylethanolamines: biological activities and metabolism. *Inflamm. Regen.* **38**, 1–10 (2018).
50. Wu, D. et al. Targeting purine metabolism-related enzymes for therapeutic intervention: A review from molecular mechanism to therapeutic breakthrough. *Int. J. Biol. Macromol.* **282**, 136828 (2024).
51. Martin-Gallausiaux, C., Marinelli, L., Blottière, H. M., Larraufie, P. & Lapaque, N. SCFA: Mechanisms and functional importance in the gut. *Proc. Nutr. Soc.* **80**, 37–49 (2021).

52. Ridlon, J. M., Kang, D. J., Hylemon, P. B. & Bajaj, J. S. Bile acids and the gut microbiome. *Curr. Opin. Gastroenterol.* **30**, 332–338 (2014).
53. Ho, A. H., Wong, S. & Lui, R. Topic: Nutrition and the gut-liver-brain axis. *Curr. Hepatol. Rep.* **21**, 99–110 (2022).
54. Dalile, B., Van Oudenhove, L., Vervliet, B. & Verbeke, K. The role of short-chain fatty acids in microbiota–gut–brain communication. *Nat. Rev. Gastroenterol. Hepatol.* **16**, 461–478 (2019).
55. Chen, Z. et al. The role of intestinal bacteria and gut–brain Axis in hepatic encephalopathy. *Front. Cell. Infect. Microbiol.* **10**, 595759 (2021).
56. Sivaprakasam, S., Prasad, P. D. & Singh, N. Benefits of short-chain fatty acids and their receptors in inflammation and carcinogenesis. *Pharmacol. Ther.* **164**, 144–151 (2016).
57. Magnusson, M. K., Isaksson, S. & Öhman, L. The anti-inflammatory immune regulation induced by butyrate is impaired in inflamed intestinal mucosa from patients with ulcerative colitis. *Inflammation* **43**, 507–517 (2020).
58. Fiorucci, S. et al. Bile acid signaling in inflammatory bowel diseases. *Digest. Dis. Sci.* **66**, 674–693 (2021).
59. Harishankar, M., Sasikala, C. & Ramya, M. Efficiency of the intestinal bacteria in the degradation of the toxic pesticide, chlorpyrifos. *3 Biotech* **3**, 137–142 (2013).
60. Velmurugan, G. et al. Gut microbial degradation of organophosphate insecticides-induces glucose intolerance via gluconeogenesis. *Genome Biol.* **18**, 1–18 (2017).
61. Reygner, J. et al. Changes in composition and function of human intestinal microbiota exposed to chlorpyrifos in oil as assessed by the SHIME® model. *Int. J. Environ. Res. Public Health* **13**, 1088 (2016).
62. Kan, H., Zhao, F., Zhang, X.-X., Ren, H. & Gao, S. Correlations of gut microbial community shift with hepatic damage and growth inhibition of Carassius auratus induced by pentachlorophenol exposure. *Environ. Sci. Technol.* **49**, 11894–11902 (2015).
63. Dechartres, J. et al. Glyphosate and glyphosate-based herbicide exposure during the peripartum period affects maternal brain plasticity, maternal behaviour and microbiome. *J. Neuroendocrinol.* **31**, e12731 (2019).
64. Tu, P. et al. Subchronic low-dose 2, 4-D exposure changed plasma acylcarnitine levels and induced gut microbiome perturbations in mice. *Sci. Rep.* **9**, 4363 (2019).
65. Wang, X., Shen, M., Zhou, J. & Jin, Y. Chlorpyrifos disturbs hepatic metabolism associated with oxidative stress and gut microbiota dysbiosis in adult zebrafish. *Comp. Biochem. Physiol. Part C: Toxicol. Pharmacol.* **216**, 19–28 (2019).
66. Kakumanu, M. L., Reeves, A. M., Anderson, T. D., Rodrigues, R. R. & Williams, M. A. Honey bee gut microbiome is altered by in-hive pesticide exposures. *Front. Microbiol.* **7**, 1255 (2016).
67. Tang, Q., Tang, J., Ren, X. & Li, C. Glyphosate exposure induces inflammatory responses in the small intestine and alters gut microbial composition in rats. *Environ. Pollut.* **261**, 114129 (2020).
68. Liu, Q. et al. Organochloride pesticides modulated gut microbiota and influenced bile acid metabolism in mice. *Environ. Pollut.* **226**, 268–276 (2017).
69. Nasuti, C. et al. Changes on fecal microbiota in rats exposed to permethrin during postnatal development. *Environ. Sci. Pollut. Res.* **23**, 10930–10937 (2016).
70. Russo, R. et al. Gut-brain axis: role of lipids in the regulation of inflammation, pain and CNS diseases. *Curr. Med. Chem.* **25**, 3930–3952 (2018).
71. Pan, X. et al. Metabolomic profiling of bile acids in clinical and experimental samples of Alzheimer's disease. *Metabolites* **7**, 28 (2017).
72. Quinn, M. et al. Bile acids permeabilize the blood brain barrier after bile duct ligation in rats via Rac1-dependent mechanisms. *Digest. Liver Dis.* **46**, 527–534 (2014).
73. Zhang, D. et al. Short-chain fatty acids in diseases. *Cell Commun. Signal.* **21**, 212 (2023).
74. Jiang, Z. et al. The gut microbiota-bile acid axis links the positive association between chronic insomnia and cardiometabolic diseases. *Nat. Commun.* **13**, 3002 (2022).
75. Jones, N. et al. Fructose reprogrammes glutamine-dependent oxidative metabolism to support LPS-induced inflammation. *Nat. Commun.* **12**, 1209 (2021).
76. Everard, A. et al. Intestinal epithelial N-acylphosphatidylethanolamine phospholipase D links dietary fat to metabolic adaptations in obesity and steatosis. *Nat. Commun.* **10**, 457 (2019).
77. Zimmermann, M., Zimmermann-Kogadeeva, M., Wegmann, R. & Goodman, A. L. Mapping human microbiome drug metabolism by gut bacteria and their genes. *Nature* **570**, 462–467 (2019).
78. Chen, L. et al. Accurate and reliable quantitation of short chain fatty acids from human feces by ultra high-performance liquid chromatography-high resolution mass spectrometry (UPLC-HRMS). *J. Pharm. Biomed. Anal.* **200**, 114066 (2021).
79. Hill, E. B. et al. Facilitating a high-quality dietary pattern induces shared microbial responses linking diet quality, blood pressure, and microbial sterol metabolism in caregiver-child dyads. *Gut Microbes* **14**, 2150502 (2022).
80. Chen, L. et al. Dairy milk casein and whey proteins differentially alter the postprandial lipidome in persons with prediabetes: A comparative lipidomics study. *J. Agric. food Chem.* **70**, 10209–10220 (2022).
81. Shen, X. et al. TidyMass an object-oriented reproducible analysis framework for LC–MS data. *Nat. Commun.* **13**, 4365 (2022).

Acknowledgements

This study was supported by the National Institute of General Medical Sciences of the National Institutes of Health (R35GM133510, to J.Z.).

Author contributions

Conceptualization, L.C. and J.Z.; Methodology, L.C., J.Z., H.Y. S.D., and Y.W.; Investigation, L.C., C.G., H.Z., A.G., S.Z., D.W., M.H., C.J., and X.W.; Writing-Original Draft, L.C. and J.Z.; Visualization, L.C. and A.G.; Funding Acquisition, J.Z.

Competing interests

The authors declare no competing interests.

Additional information

Supplementary information The online version contains supplementary material available at https://doi.org/10.1038/s41467-025-59747-6.

Correspondence and requests for materials should be addressed to Jiangjiang Zhu.

Peer review information *Nature Communications* thanks Robin Mesnage, Wells Utembe, and the other, anonymous, reviewers for their contribution to the peer review of this work. A peer review file is available.